A Mathematical Analysis of the Generation and Termination of Calcium Sparks

R. Hinch
University Laboratory of Physiology and Oxford Centre for Industrial and Applied Mathematics, Mathematical Institute, University of Oxford, Oxford, United Kingdom

ABSTRACT Calcium sparks are local regenerative releases of Ca^{2+} from a cluster of ryanodine receptors on the sarcoplasmic reticulum. During excitation-contraction coupling in cardiac cells, Ca^{2+} sparks are triggered by Ca^{2+} entering the cell via the T-tubules (Ca^{2+}-induced Ca^{2+} release). However under conditions of calcium overload, Ca^{2+} sparks can be triggered spontaneously. The exact process by which Ca^{2+} sparks terminate is still an open question, although both deterministic and stochastic processes are likely to be important. In this article, asymptotic methods are used to analyze a single Ca^{2+} spark model, which includes both deterministic and stochastic biophysical mechanisms. The analysis calculates both spark frequencies and spark duration distributions, and shows under what circumstances stochastic transitions are important. Additionally, a model of the coupling of the release channels via the FK-binding protein is analyzed.

INTRODUCTION

Cardiac myocytes contract when the intracellular Ca^{2+} concentration is raised from its resting level of from ~100 nM to 1000 nM. The majority of this Ca^{2+} is released from the sarcoplasmic reticulum (SR) through the ryanodine receptors (RyRs) (Franzini-Armstrong et al., 1998, 1999). The RyRs are situated in clusters of 10–100 on the surface of the SR close to the T-tubules. L-type Ca^{2+} channels (LCCs) are located on the T-tubules facing each cluster of RyRs. The region between the SR and T-tubule is called the diadic space (or subspace or fuzzy space); note that there are many diadic spaces per cell (Lederer et al., 1990; Soeller and Cannell, 1997). The part of the SR in the vicinity of the RyRs is called the junctional SR (JSR); note that the local $[Ca^{2+}]$ in the JSR can be different to that in the bulk SR. The diadic space, JSR, RyRs, and LCCs make up a Ca^{2+} release unit (CaRU). During excitation-contraction coupling, Ca^{2+} release from the SR is triggered by a small influx of Ca^{2+} through the LCCs into some of the diadic spaces (Cheng et al., 1994; Shacklock et al., 1995). This Ca^{2+} then binds with RyRs causing them to open and triggering a much larger Ca^{2+} current from the SR. This process is locally regenerative in that it displays positive feedback. As more RyRs open, the current from SR increases and the local $[Ca^{2+}]$ in the diadic space increases. This in turn increases the number of RyRs that Ca^{2+} binds with, thus further increasing the current from the SR. This feedback is local in that it acts within a single CaRU and forms the basis of local control models of the Ca^{2+} release (Niggli and Lederer, 1990). Local control models have the advantage over common pool models in that they display both high gain and graded release (Stern, 1992; Greenstein and Winslow, 2002). Calcium sparks are spontaneous localized releases of Ca^{2+} from the SR (Cheng et al., 1993; Lopez-Lopez et al., 1994).

The process by which Ca^{2+} release from the SR is terminated is still open, but four distinct hypotheses have been proposed:

1. Stochastic attrition. This is when all the RyRs in CaRU shut spontaneously by chance (Stern, 1992). Although it has been demonstrated that this cannot be the sole mechanism for spark termination (Stern et al., 1999), we believe it is an important modulating factor.
2. Total local depletion of JSR. This is when the $[Ca^{2+}]$ in the JSR in the vicinity of the RyRs drops to zero (Varro et al., 1993; Bassani et al., 1995; Negretti et al., 1995). Again this has been contradicted by experiments showing the existence of long sparks (Cheng et al., 1993) and nonzero SR Ca^{2+} content directly after Ca^{2+} release. However, these experiments do not contradict the hypothesis that the local JSR $[Ca^{2+}]$ is partially reduced.
3. RyR channel inactivation. This is when the RyRs are closed due to a Ca^{2+}-dependent or time-dependent inactivation (Gyorke and Fill, 1993; Zahradnikova and Zahradnik, 1996). Experiments on isolated RyRs suggest that this process occurs too slowly or not sufficiently to account for spark termination (Gyorke and Fill, 1993; Nabauer and Morad, 1990). However, it should be noted that the rate of inactivation is modulated by Mg^{2+} and adenine nucleotides (Valdivia et al., 1995; Xu et al., 1996). There is some experimental evidence suggesting that RyR inactivation plays a role in spark termination (Sham et al., 1998), however, these experiments failed to exclude that partial SR depletion is the predominant mechanism of spark termination. RyR channel inactivation is not used in our model.
4. RyR sensitivity to JSR Ca^{2+}. Experiments have shown that RyRs in cardiac cells become less sensitive to Ca^{2+} in the diadic space when JSR Ca^{2+} is depleted (Cheng et al., 1996; Lukyanenko et al., 1998; Thedford et al.,

Submitted May 21, 2003, and accepted for publication October 20, 2003

Address reprint requests to Dr. Robert Hinch, E-mail: hinch@maths.ox.ac.uk.

0006-3495/04/03/1293/15 $2.00

1994; Gyorke and Gyorke, 1998; Ching et al., 2000; Terentyev et al., 2002). For this mechanism to be important, JSR [Ca^{2+}] must be partially depleted during a spark.

In addition to these four principle mechanisms of termination, experiments have shown that the cooperation between RyRs in the CaRU can effect the process of spark termination. Each RyR is linked to its four nearest neighbors by an FK-binding protein (FKBP), which couples the gating of the channel (Wagenknecht et al., 1997; Marx et al., 2001). Removal of this protein using FK506 dramatically increases the length of sparks (Xiao et al., 1997; Lukyanenko et al., 1998). A recent model incorporating the effect of FKBP has shown in principle that spark length can be increased by inhibiting this protein (Sobie et al., 2002). A mathematical analysis will be used to determine the origin of this change in behavior.

In this article, a model of a CaRU is presented and the Ca^{2+} sparks that it generates are analyzed. The model includes:

1. Separate compartments for the bulk cytoplasm, diadic space, JSR, and network SR (NSR).
2. A stochastic model of the RyRs that includes coupled gating and sensitivity to JSR Ca^{2+}. Each CaRU contains a cluster of RyRs.
3. Ca^{2+} buffers in the diadic space and the JSR (i.e., calmodulin and calsequestrin).

These different biophysical processes occur over a vast range of timescales that can be exploited using an asymptotic analysis to simplify the model. Asymptotic analysis is a branch of mathematics that allows approximate solutions to be found in the limit that a parameter in the model is small (in this case, the ratio of two different biophysical timescales). This greatly simplifies the system of equations to be solved; however, they still remain stochastic. The stochastic behavior is analyzed by taking advantage of the large number of receptors in the cluster (10–100). Two macroscopic states can then be used to describe the ensemble of RyRs, one when most of the receptors are closed and one when most of the receptors are open. A new asymptotic technique is then used to calculate the rate of transitions between these two macroscopic states. The technique of stochastic phase-plane analysis is then used to analyze the distribution of spark lengths (Hinch, 2002). Spark frequencies and the effect of FK506 are also analyzed. The results of the analysis are compared with Monte Carlo numerical simulations of the model and experimental observations.

Ca^{2+} SPARK MODEL

In this section, the elements and equations of the model are described. Fig. 1 is a schematic diagram of the CaRU and the position of the different compartments and receptors. The

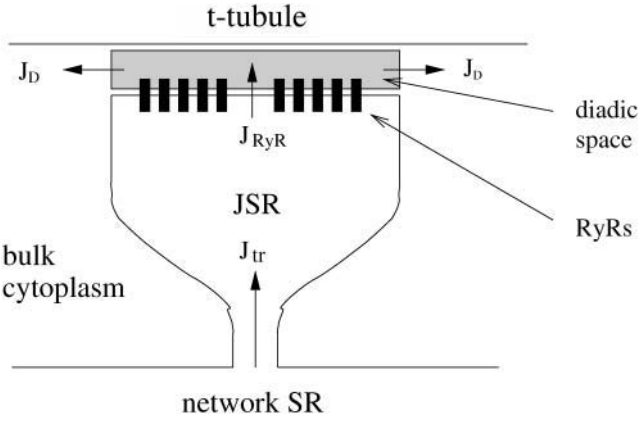

FIGURE 1 Components of the CaRU used in the model. The model includes four separate compartments: the network SR, the junctional SR, the diadic space, and the bulk myoplasm.

diadic space is the thin region of the cytoplasm between the JSR and the T-tubules. The geometry of the diadic space can be approximated by a cylinder of height 10 nm and radius 200 nm (Frank, 1990), giving it a volume (V_{ds}) of 1.26×10^{-3} μm^3. This is a very small volume, especially when we consider the typical [Ca^{2+}] in the space (~ 1 μM). A simple calculation then reveals that the expected number of ions in the space is ~ 1. This raises questions about the validity of using a concentration to describe the Ca^{2+} in the space and using the diffusion equation to model the transport of Ca^{2+} within the diadic space. These issues have not previously been addressed in spark models and are not addressed in this article. The faces of the cylinder represent the surface of the SR and T-tubule, and Ca^{2+} can diffuse through the sides into the bulk cytoplasm. The diadic space contains Ca^{2+} buffers such as calmodulin. The Ca^{2+} concentration in the diadic space ($[Ca^{2+}]_{ds}$) is given by

$$V_{ds}\frac{d[Ca^{2+}]_{ds}}{dt} = J_{RyR} - J_D + \frac{V_{ds}}{\tau_B}\left([BCa^{2+}]_{ds} - \frac{[Ca^{2+}]_{ds}[B]_{ds}}{K_B}\right), \quad (1)$$

the concentration of the buffer is given by

$$\frac{d[B]_{ds}}{dt} = \frac{1}{\tau_B}\left([BCa^{2+}]_{ds} - \frac{[Ca^{2+}]_{ds}[B]_{ds}}{K_B}\right), \quad (2)$$

and the total buffer concentration in the diadic space is conserved

$$[BCa^{2+}]_{ds} + [B]_{ds} = [B]_{tot}, \quad (3)$$

where J_{RyR} is the total current into the diadic space through the RyRs, J_D is the diffusive current from the diadic space into the bulk cytoplasm, $[B]_{ds}$ is the concentration of the buffer in the diadic space, $[BCa^{2+}]_{ds}$ is the concentration of the Ca^{2+} –buffer complex in the diadic space, $[B]_{tot}$ is the total buffer concentration in the diadic space, τ_B is the buffering time constant, and K_B is the buffer-Ca^{2+}

dissociation constant. A glossary of parameters and estimates of their values using experimental measurements can be found in Appendix 2. The diffusive Ca^{2+} current from the diadic space is modeled by

$$J_D = g_D([Ca^{2+}]_{ds} - [Ca^{2+}]_{myo}), \quad (4)$$

where $[Ca^{2+}]_{myo}$ is the myoplasmic Ca^{2+} concentration, which is held constant, and g_D is the rate of diffusion form the diadic space. The constant g_D can be approximated by considering the area of interface between the diadic space and the bulk myoplasm, the diffusion coefficient for Ca^{2+}, and an effective diffusion length. The timescale over which $[Ca^{2+}]_{ds}$ reaches its equilibrium value is then given by $\tau_{ds} = V_{ds}/g_D \approx 1.66 \times 10^{-3}$ ms (see Appendix 2). Note that this timescale is much quicker than the timescale of the buffering of Ca^{2+} to calmodulin and the open time of the RyRs. This approximation agrees with previous estimates of τ_{ds} (Sobie et al., 2002). The Ca^{2+} concentration in the JSR ($[Ca^{2+}]_{JSR}$) is given by

$$\frac{d[Ca^{2+}]_{JSR}}{dt} = \beta_{JSR}\left(-\frac{J_{RyR}}{V_{JSR}} + \frac{[Ca^{2+}]_{NSR} - [Ca^{2+}]_{JSR}}{\tau_{tr}}\right), \quad (5)$$

where τ_{tr} is the transfer rate from the network SR to the JSR, and β_{JSR} is the buffering factor due to calsequestrin calculated using the rapid buffering approximation (Wagner and Keizer, 1994)

$$\beta_{JSR} = \left(1 + \frac{[CSQ]_{total}K_{CSQ}}{(K_{CSQ} + [Ca^{2+}]_{JSR})^2}\right)^{-1}. \quad (6)$$

Note that in this model, $[Ca^{2+}]_{JSR}$ is partially depleted during a spark, but does not fall to zero. The role of the buffer in the JSR is to slow the change in $[Ca^{2+}]$. For simplicity, we consider the linear buffer regime β_{JSR} to be a constant, which is approximately true when $K_{CSQ} \gg [Ca^{2+}]_{JSR}$.

Ryanodine receptors

The CaRU contains N functional RyRs. The RyRs are assumed to gate independently of each other except for the coupling factor due to the FK-binding protein (Sobie et al., 2002). Since it is believed that RyR inactivation happens too slowly to terminate sparks, we will not include activation in this model. The model of the RyRs is a simplified three-state model represented by the following reaction sequence

$$C_1 + \alpha Ca^{2+} \rightleftharpoons C_2 \rightleftharpoons O. \quad (7)$$

At low $[Ca^{2+}]$, the receptor is in the closed state C_1; when αCa^{2+} ions bind to the receptor, it is promoted to the C_2 closed state. The receptor then switches between the C_2 state and the O state representing the H-mode of RyRs (Zahradnikova and Zahradnik, 1996). The transition between the C_1 and C_2 states is assumed to be very rapid; therefore. the model can be approximated by a two-state model

$$C \rightleftharpoons O, \quad (8)$$

with transition coefficient

$$k_+ = CF_+ \frac{[Ca^{2+}]_{ds}^{\alpha}}{\rho\tau_{open}([Ca^{2+}]_{ds}^{\alpha} + K_{RyR}^{\alpha})}, \quad (9)$$

and

$$k_- = \frac{CF_-}{\tau_{open}}, \quad (10)$$

where K_{RyR} is the dissociation constant of the RyR, τ_{open} is the mean open time of the channel in the H-mode, ρ is the proportion of time the channel is closed when the receptor is in the H-mode, and $CF_\pm$ are the coupling factors (Sobie et al., 2002). The sensitivity of the RyRs on $[Ca^{2+}]_{JSR}$ is modeled by $K_{RyR} = K_0(1 - \Delta[Ca^{2+}]_{JSR})$ (Sobie et al., 2002). The model will be investigated with Hill constant $\alpha = 4$ (Sobie et al., 2002) and comparisons made with the case when $\alpha = 3$. First a model without coupling will be considered ($CF_\pm = 1$). Then a simple model including coupled-gating will be examined (Sobie et al., 2002) with

$$CF_+ = 1 + \phi, \quad (11)$$

and

$$CF_- = k_{coup}(1 + \phi), \quad (12)$$

where ϕ is the proportion of the receptors in the open state. One problem with this simple model of coupling is that the coupling factor k_{coup} multiplies the open probability of the RyRs, which shifts their overall sensitivity. However, this model has successfully reproduced experimental results of interrupting the RyR coupling (Sobie et al., 2002). Finally the total current through all the RyRs is given by

$$J_{RyR} = J_{max}\phi\frac{[Ca^{2+}]_{JSR} - [Ca^{2+}]_{ds}}{[Ca^{2+}]_{NSR}}, \quad (13)$$

where J_{max} is the maximum current when all RyRs are open and $[Ca^{2+}]_{JSR}$ has not been depleted. J_{max} can be estimated by dividing the total flux of Ca^{2+} released by each CaRU during E-C coupling by the mean release time. In the modeling in this article we will assume that J_{max} is independent of the number of receptors in the CaRU.

MATHEMATICAL ANALYSIS

The model described in the previous section contains a stochastic model of a group of RyRs coupled to three differential equations to describe the $[Ca^{2+}]$ in the different compartments. Although it is simple to solve this model numerically using Monte Carlo simulations, it can be simplified using asymptotic analysis. The model contains a wide range of biophysical timescales. By taking advantage of the

large ratios of these timescales, the three differential equations can be simplified to one. The second large number in the model is the number of RyRs (N) in the CaRU (10–100). A novel asymptotic mathematical technique taking advantage of the fact that $N \gg 1$ is then used to simplify the model of the cluster of RyRs. This analysis allows us to consider the entire cluster as a two-state stochastic model, where either all the RyRs are shut or most of them are open. These approximations can then be used to calculate analytical expressions for the distributions of spark termination times and spark frequencies.

Multiple timescales

The first step in the problem is to nondimensionalize the equations. This process allows us to clearly identify the different biophysical timescales. Define the nondimensional parameters

$$t' \equiv \frac{t}{\tau_{\text{open}}}, \quad C \equiv \frac{[\text{Ca}^{2+}]_{\text{ds}}}{K_0} \quad \text{and} \quad J \equiv \frac{J_{\max}}{g_{\text{D}} K_0} \frac{[\text{Ca}^{2+}]_{\text{JSR}}}{[\text{Ca}^{2+}]_{\text{NSR}}}, \quad (14)$$

and the nondimensional parameters

$$\varepsilon_{\text{ds}} \equiv \frac{\tau_{\text{ds}}}{\tau_{\text{open}}}, \quad \varepsilon_{\text{B}} \equiv \frac{\tau_{\text{ds}}}{\tau_{\text{B}}}, \quad \varepsilon_{\text{m}} \equiv \frac{[\text{Ca}^{2+}]_{\text{myo}}}{K_0},$$

$$\varepsilon_{\text{JSR}} \equiv \frac{J_{\max}}{g_{\text{D}}[\text{Ca}^{2+}]_{\text{NSR}}}, \quad J_0 \equiv \frac{J_{\max}}{g_{\text{D}} K_0}, \quad \delta \equiv \frac{\Delta g_{\text{D}} K_0 [\text{Ca}^{2+}]_{\text{NSR}}}{J_{\max}},$$

$$\tau_{\text{JSR}} \equiv \frac{[\text{Ca}^{2+}]_{\text{NSR}} V_{\text{JSR}}}{\tau_{\text{open}} \beta_{\text{JSR}} J_{\max}}, \quad \text{and} \quad r \equiv \frac{\tau_{\text{JSR}} \tau_{\text{open}} \beta_{\text{JSR}}}{\tau_{\text{tr}}}. \quad (15)$$

Values for these nondimensional parameters are given in Appendix 2. The parameters $\varepsilon_{\text{i}} \ll 1$ and $\tau_{\text{JSR}} \gg 1$; these relative sizes in parameters will be exploited in the asymptotic analysis. The separation of physiological timescales that leads to these small parameters are:

1. ε_{ds}, the mean open time of a RyR is much longer than the rate at which $[\text{Ca}^{2+}]_{\text{ds}}$ equilibrates after a change in the current into the diadic space.
2. ε_{B}, the rate at which Ca^{2+} buffers to calmodulin rate is much slower than the rate at which $[\text{Ca}^{2+}]_{\text{ds}}$ equilibrates after a change in the current into the diadic space.
3. ε_{m}, the resting myoplasmic $[\text{Ca}^{2+}]$ is much less than the dissociation constant of the RyR.
4. ε_{JSR}, the $[\text{Ca}^{2+}]$ in the diadic space is much lower than the $[\text{Ca}^{2+}]$ in the JSR.
5. τ_{JSR}, the time over which Ca^{2+} is depleted in the JSR during a spark is much longer than the individual mean open time of a RyR.

These differences in timescales will be used in the asymptotic analysis by calculating approximate solutions in the limit $\varepsilon_{\text{i}} \searrow 0$ and $\tau_{\text{JSR}} \nearrow \infty$. The nondimensional equation for the rate of change of $[\text{Ca}^{2+}]_{\text{ds}}$ is

$$\varepsilon_{\text{ds}} \frac{dC}{dt'} = J\phi \left(1 - \varepsilon_{\text{JSR}} \frac{C}{J}\right) - (C - \varepsilon_{\text{m}}) + \varepsilon_{\text{B}} \left(\frac{[\text{BCa}^{2+}]_{\text{ds}}}{K_0} - \frac{C[\text{B}]_{\text{ds}}}{K_{\text{B}}}\right), \quad (16)$$

and for the rate of change of $[\text{Ca}^{2+}]_{\text{JSR}}$ is

$$\tau_{\text{JSR}} \frac{dJ}{dt'} = -J\phi + r(J_0 - J). \quad (17)$$

Simple asymptotic analysis tell us that the solution of Eq. 16 in the limit $\varepsilon_{\text{B}}, \varepsilon_{\text{JSR}}, \varepsilon_{\text{ds}} \searrow 0$ is

$$C \sim J\phi + \varepsilon_{\text{m}}. \quad (18)$$

The physiological meaning of this result is that the $[\text{Ca}^{2+}]_{\text{ds}}$ is proportional to the current entering the space from the JSR plus the $[\text{Ca}^{2+}]_{\text{myo}}$. When we model spark termination, the ε_{m} term is dropped since it is small during a spark (i.e., $J\phi \gg \varepsilon_{\text{m}}$). However, when we model the spontaneous generation of sparks, it is necessary to retain it, since before a spark there is no current from the JSR into the diadic space (i.e., $J\phi < \varepsilon_{\text{m}}$ since $\phi = 0$). Nondimensionalizing the transition rates for the individual RyRs and using Eq. 18 gives

$$k_+ = \frac{\text{CF}_+ (J\phi + \varepsilon_{\text{m}})^{\alpha}}{\rho((1 - \delta J)^{\alpha} + (J\phi + \varepsilon_{\text{m}})^{\alpha})} \quad \text{and} \quad k_- = \text{CF}_-. \quad (19)$$

Stochastic fixed-point transitions

The dynamics of the model are determined by solving the stochastic Eq.19 for the opening and closing of the RyRs and the differential Eq.17 for the change in Ca^{2+} in the JSR. First we shall consider the simplified problem when the $[\text{Ca}^{2+}]_{\text{JSR}}$ (J) is constant. The opening and closing of the individual RyRs is independent, with the exception that the transition rates are a function of the proportion of the RyRs in the open state (ϕ). This then allows the cluster of the RyRs to be represented by an $N + 1$ state continuous time Markov chain with jump functions

$$f_{\text{n}} = N(1 - \phi)k_+ \quad \text{and} \quad g_{\text{n}} = N\phi k_-, \quad (20)$$

where n is the number of RyRs in the open state, f_{n} is the jump function from the n to $n + 1$ position on the chain, and g_{n} is the jump function from the n to $n - 1$ position on the chain. Note that $\phi = n/N$, and f_{n} and g_{n} are functions of both ϕ and J. Now we consider the behavior of this chain in the limit $N \nearrow \infty$, i.e., a large number of RyR in the cluster (Hinch, 2002). The discrete jump functions f_{n} and g_{n} can be represented by continuous functions $f(\phi)$ and $g(\phi)$. The chain has stationary points (similar to fixed points in differential equations) where $f(\phi^*) = g(\phi^*)$. The stationary points will be stable if $g'(\phi^*) > f'(\phi^*)$, where $' \equiv \text{d}/\text{d}\phi$. In the limit $N \nearrow \infty$, the system will remain in the region of the chain close to a stable stationary point. If the chain has one

stable stationary point, the steady-state distribution will form an approximate Gaussian of width order $1/\sqrt{N}$ (written as $O(1/\sqrt{N})$) centered on the stable stationary point (Hinch, 2002). If the system has two stable stationary points (there will be an intermediate unstable stationary point on the chain with $g'(\phi^*) < f'(\phi^*)$), then it will remain in the region of one the stationary points for long periods of times (dwell times). It will then make a stochastic transition between the two stable stationary points (an example of such transitions is shown in Fig. 2, see below). The mean first passage time is the mean time between the switching between the stable stationary points. Consider a chain with two stable stationary points, ϕ_- and ϕ_+, and one unstable stationary point, ϕ_0, such that $\phi_- < \phi_0 < \phi_+$. An asymptotic calculation of the mean first passage time of stochastic fixed-point transition from ϕ_+ to ϕ_- in the limit $N \nearrow \infty$ is given by (see Appendix 1, Eq. 52, and Hinch, 2002)

$$\tau_{\text{term}} = \exp(N\Delta V_+)\left(\frac{2\pi N}{f(\phi_+)\sqrt{-\gamma(\phi_0)\gamma(\phi_+)}} + O(1)\right), \tag{21}$$

where $\Delta V_+ = V(\phi_0) - V(\phi_+)$,

$$V(\phi) = \int^{\phi} \ln\left(\frac{g(\phi')}{f(\phi')}\right) d\phi', \tag{22}$$

and

$$\gamma(\phi) = \frac{g'}{g} - \frac{f'}{f}. \tag{23}$$

Here $V(\phi)$ is the ''derived potential'' of the chain. This expression for the mean first passage times is of a similar form to Kramers' formula for the transition times of a particle in a double potential well due to thermal fluctuations (Kramers, 1940). The mean first passage times can now be used to calculate the rate of spark terminations due to stochastic attrition. When the JSR loading is sufficiently large, the chain has two stable stationary points. ϕ_+ is the stable stationary point where most of the receptors are open (i.e., during Ca^{2+} release), and ϕ_- is the stable stationary point where most of the receptors are closed. Fig. 2 shows two typical time series of the position on the chain calculated using a Monte Carlo simulation. Note that the system remains in the region of ϕ_+ for a long time before suddenly jumping to ϕ_-, and that in the two simulations this time is different. The first passage times form an exponential distribution since the rate of a stochastic fixed-point transition is constant. A comparison of the mean first passage time calculated using the Monte Carlo simulation and using the asymptotic analysis (Eq. 21) is shown in Fig. 2 *C*. The figure shows the mean first passage time as a function of the number of receptors in the cluster (N) for four different values of JSR loading. The mean first passage time was calculated by averaging the results of 1000 ''sparks'' (remember these are not solutions of the full spark model since the local JSR Ca^{2+} is constant). As N is increased, the error in asymptotic calculation is reduced and the mean spark duration increases rapidly. The result confirms that stochastic transition cannot be the only mechanism responsible for spark termination.

Equation 21 for the stochastic termination of a spark (τ_{stoch}) is invalid when we consider stochastic spark generation. This is because for the majority of the time when a spark is not occurring, all the RyRs are closed. Therefore the stationary point on the chain is very close to $\phi = 0$ and the discreteness individual states of the chain must be considered. The asymptotic analysis can be modified to yield (see Appendix 1, Eq. 53)

$$\tau_{\text{gen}} = \exp(N\Delta V_-) \times \left(\frac{g(1/N)\sqrt{2\pi N}}{\Gamma f(0)\sqrt{-\gamma(\phi_-)f(1/N)g(1/N)}} + O\left(1/\sqrt{N}\right)\right), \tag{24}$$

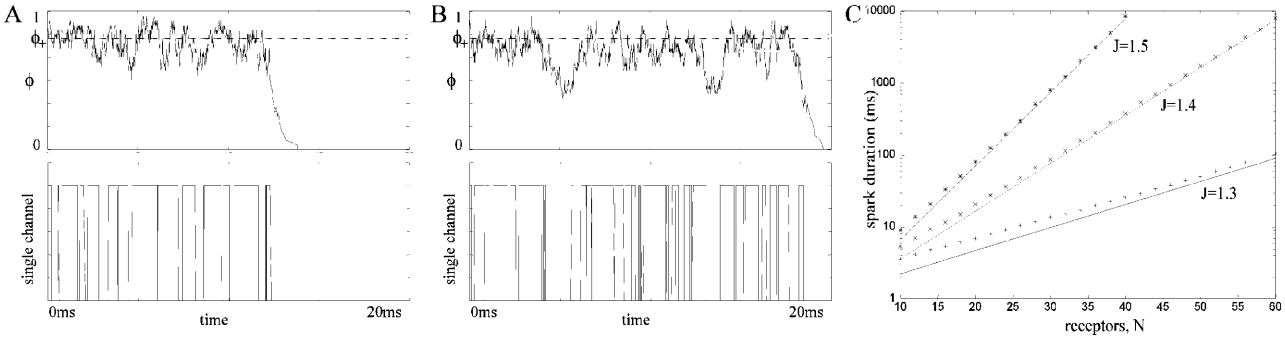

FIGURE 2 (*A* and *B*) Monte Carlo simulations of proportion of RyRs in the open state and the transitions of one of the RyRs in the cluster. Note that the proportion of the receptors in the open state remains in the region of the stable stationary point ϕ_+ before making a rapid transition to the stable stationary point $\phi_- = 0$. (*C*) The mean spark time as a function of the number of receptors in the cluster for the constant JSR Ca^{2+} model. The line is the asymptotic calculation and the points are from a Monte Carlo simulation. Note that the spark time is a log scale. As the number of receptors in the cluster increases, the spark time increases and the error in asymptotic calculation decreases. The mean spark length also increases rapidly with JSR loading J. The model parameters used where $\alpha = 4$, $\varepsilon_m = 0$, and $\rho = 0.2$.

where $\Delta V_- = V(\phi_0) - V(1/N)$. This equation is used later to calculate spark frequencies.

Stochastic phase-plane analysis

The analysis is now extended to consider the dynamics of J, which is governed by the differential Eq. 17 and is a function of both ϕ and J. The technique combines the theory of stochastic transition in the previous section with deterministic phase-plane analysis used to analyze systems such as the FitzHugh-Nagumo model (FNM) (Keener and Sneyd, 1998). In the FNM, there is a fast variable and a slow variable. The timescale over which J varies is much slower than the timescale over stochastic variable ϕ varies since $\tau_{\mathrm{JSR}} \gg 1$. Therefore J will act like the slow variable in the FNM and ϕ like the fast variable. In the FNM this separation in timescales means that the system remains in the region of the nullclines of ϕ, so that ϕ in the differential equation for J (Eq. 17) can be replaced by the value on the nullcline (calculated by solving for $\mathrm{d}\phi/\mathrm{d}t = 0$). However, in the spark model, ϕ is a stochastic variable described by a Markov process. Instead of using the value on the nullcline, we use the value at the stationary point on the chain $\phi_\pm(J)$. A simple justification of this procedure can be seen by considering a local time averaged value of ϕ during a spark (when the system is in the vicinity of the stationary point $\phi_+(J)$). The time average of ϕ over a time τ_{LA} where $1 \ll \tau_{\mathrm{LA}} \ll \tau_{\mathrm{JSR}}$ is

$$\phi(t) \approx \frac{1}{\tau_{\mathrm{LA}}}\int_{t-\tau_{\mathrm{LA}}/2}^{t+\tau_{\mathrm{LA}}/2} \phi\,\mathrm{d}t' \approx \phi_+(J), \tag{25}$$

which is simply the stable stationary point during a spark (a full justification of this procedure is included in Hinch, 2002). Inserting this time-averaged value of the fast variable ϕ into Eq. 17 yields

$$\tau_{\mathrm{JSR}}\frac{dJ}{dt} = -J\phi(J) + r(J_0 - J). \tag{26}$$

Fig. 3 *B* shows $J(t)$ calculated for a spark using Eq. 26 and from a Monte Carlo simulation of the model. The two are in excellent agreement, confirming the validity of this approximation. The nullclines of the spark model are shown in Fig. 3 *A* along with a sample spark calculated using a Monte Carlo simulation. In deterministic phase-plane analysis, a spark is generated when the system is excited from its global fixed point (*1*) to the nullcline $\phi_+(J)$ (*2*). J would then decrease after the nullcline $\phi_+(J)$ until it "falls off" at $J = J_c$ (*3*) where the nullcline disappears. The system would then jump back to the nullcline $\phi_-(J)$. However, we see that the sample spark in Fig. 3 *A* terminates before $J = J_c$ due to a stochastic fixed-point transition. The rate of termination of sparks due to stochastic transitions is (Eq. 21)

$$k_{\mathrm{term}}(t) = \frac{1}{\tau_{\mathrm{term}}(t)} \approx \frac{f(\phi_+(J))\sqrt{-\gamma(\phi_0(J))\gamma(\phi_+(J))}}{2\pi N} \times \exp(-N\Delta V_+), \tag{27}$$

where $\Delta V_+ = V(\phi_0(J)) - V(\phi_+(J))$, and J is given by the solution of Eq. 26. The final step is to calculate the distribution of spark durations. Let T be a random variable drawn from the distribution of spark durations, $P(T > \tau)$ be the probability that a spark is longer than τ, and $p(\tau)$ be the probability density function of spark durations. The probability that a spark terminates in an infinitesimal time interval $\delta\tau$ is simply $k_{\mathrm{term}}(\tau)\delta\tau$, so

$$P(T > \tau + \delta\tau) = P(T > \tau)(1 - k_{\mathrm{term}}(\tau)\delta\tau) + O(\delta\tau^2). \tag{28}$$

Taking the limit $\delta\tau \searrow 0$ and integrating the resultant first order differential equation gives $P(T > \tau)$. Finally, differentiating yields

$$p(\tau) = k_{\mathrm{term}}(\tau)\exp\left(-\int_0^\tau k_{\mathrm{term}}(t)\mathrm{d}t\right). \tag{29}$$

In words, this equation says that the probability density of a spark of length τ is equal to the instantaneous rate of spark termination multiplied by a discount factor related to the probability that the spark has already terminated. This equation will be used later to calculate the distribution of spark durations.

RESULTS OF MODEL

The mathematical analysis outlined in the previous section will now be applied to three examples of the local release of

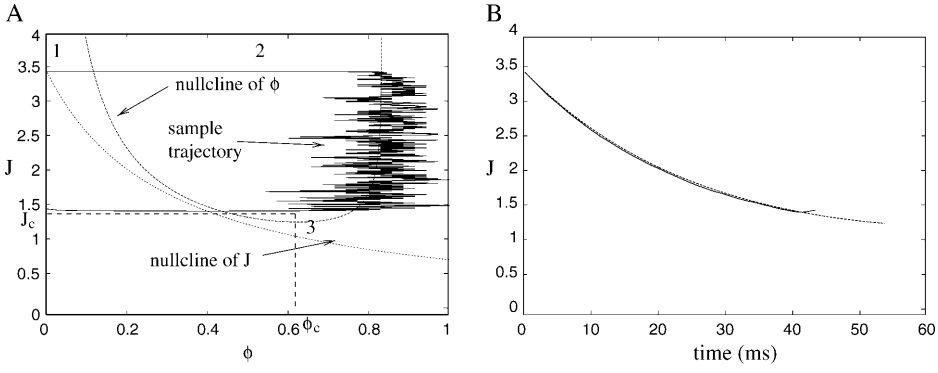

FIGURE 3 (*A*) Phase plane and nullclines of the spark model and a sample trajectory of a spark calculated using a Monte Carlo simulation. At rest, the CaRU is at *1*; when a spark is generated, it move to the nullcline $\phi_+(J)$ (*2*), and then moves down the nullcline until it "falls off" before $J = J_c$ (*3*). Note in deterministic phase-plane analysis, it will only "fall off" the nullcline at $J = J_c$. (*B*) The value of J as a function time calculated using the asymptotic analysis (Eq. 26) and from the same Monte Carlo simulation shown in *A*.

Ca^{2+}. The results of the asymptotic analysis will be compared with Monte Carlo simulations of the model, and are shown to be in excellent agreement.

Spark frequency

Calcium sparks are observed in healthy cells with a low frequency. However, when the intracellular Ca^{2+} is increased, the frequency of spontaneous Ca^{2+} sparks is greatly increased. This suggests that Ca^{2+} sparks are related to either (or more likely both) elevated myoplasmic and SR Ca^{2+} levels. Fig. 4 *A* shows the relationship between mean spark separation (i.e., inverse of the spark frequency) and $[Ca^{2+}]_{myo}$ predicted by the model. The lines represent the results of the analysis and the points are the results of Monte Carlo simulations (averaged over 1000 sparks). The graph contains three lines, each with different SR Ca^{2+} loading (0.8 mM, 1.0 mM, and 1.2 mM). Note that the mean spark separation decreases from 10^5 s at low $[Ca^{2+}]_{myo}$ (25 nM) to 1 s at high $[Ca^{2+}]_{myo}$ (300 nM), and the relationship is highly nonlinear. This number can then be converted to a figure for the whole cell by dividing by the total number of release sites in the cell. When $[Ca^{2+}]_{myo} = 100$ nM and $[Ca^{2+}]_{JSR} = 1.0$ mM, the model predicts 10 sparks per cell per second.

Fig. 4 *B* shows the relationship between mean spark separation and $[Ca^{2+}]_{JSR}$ for a single release site. The graph contains four lines, each with different $[Ca^{2+}]_{myo}$ (50 nM, 100 nM, 150 nM, and 200 nM). Again note that the dependence of spark separation on $[Ca^{2+}]_{JSR}$ is highly nonlinear. The spark frequency increases rapidly as $[Ca^{2+}]_{myo}$ is increased. The results show that when $[Ca^{2+}]_{JSR}$ is increased to 1.2 mM and $[Ca^{2+}]_{myo}$ is increased to 150 nM, the mean sparks separation is reduced to ~10 s. This figure equates to >1000 sparks per cell per second and explains why Ca^{2+} sparks can be observed in line scan images of cells where the $[Ca^{2+}]$ is elevated. Additionally, the model shows that the spark frequency is very sensitive to changes in $[Ca^{2+}]_{JSR}$. This agrees with experimental results from cells exhibiting spontaneous Ca^{2+} waves. The frequency of Ca^{2+} sparks rapidly increases between waves as the SR Ca^{2+} store is slowly replenished (Aptel and Freestone, 1998).

The model can be used to calculate the relationship between the spark frequency and the number of RyRs in the cluster. The maximum Ca^{2+} current from the JSR (i.e., when all the RyRs open) is kept constant when the number of RyRs is varied. Fig. 4 *C* shows the relationship between the mean spark separation and the number of RyRs in the cluster for a single release site. Note that as the number of RyRs increases, the spark frequency is reduced rapidly. The graph shows the results for two different exponents of the RyR model ($\alpha = 3$ and $\alpha = 4$). This exponent is the number of Ca^{2+} ions that need to bind to the receptor to ''open'' it. When the exponent is reduced from $\alpha = 4$ (default value, Sobie et al., 2002) to $\alpha = 3$, the spark frequency increases by a factor of >1000. The results of this model are only consistent with experimental observations of sparks if we use the exponent $\alpha = 4$.

Termination of sparks

In this section, the mechanism for the termination of Ca^{2+} release is investigated, and the relative importance of stochastic attrition and partial depletion of the JSR is examined. The distribution of spark durations can be calculated using Monte Carlo simulations and by using ''stochastic phase-plane analysis'' (see that section earlier). Fig. 5 shows the distribution of spark durations predicted by the model for different numbers of RyRs in the CaRU. When there are 10 RyRs in the CaRU, the distribution of sparks is a bell-shaped curve centered on a release duration of 14 ms with width 10 ms. When the number of RyRs is increased to 40 in the CaRU, the distribution is a bell-shaped curve centered on a release duration of 20 ms with width 5 ms. The difference is due to the relative importance of stochastic

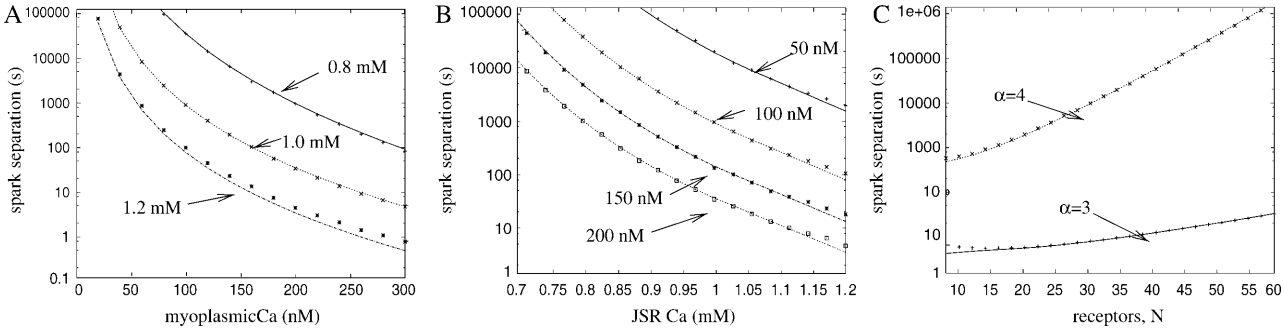

FIGURE 4 (*A*) Mean spark separation as a function of myoplasmic Ca^{2+} concentration ($\int_m$) for three different levels of JSR Ca^{2+} loading. (*B*) Mean spark separation as a function of JSR Ca^{2+} concentration (*J*) for four different levels of myoplasmic Ca^{2+} concentration. (*C*) Mean spark separation as a function of the number of RyRs in the cluster (*N*). The graph shows the results for different exponents in the RyR model ($\alpha = 3$ and $\alpha = 4$). The dots are the results of Monte Carlo simulations and the lines are the prediction of the analysis. Note that the timescale is a log scale. The default values are 40 RyRs, 100 nM of myoplasmic Ca^{2+}, and 1 mM of JSR Ca^{2+}.

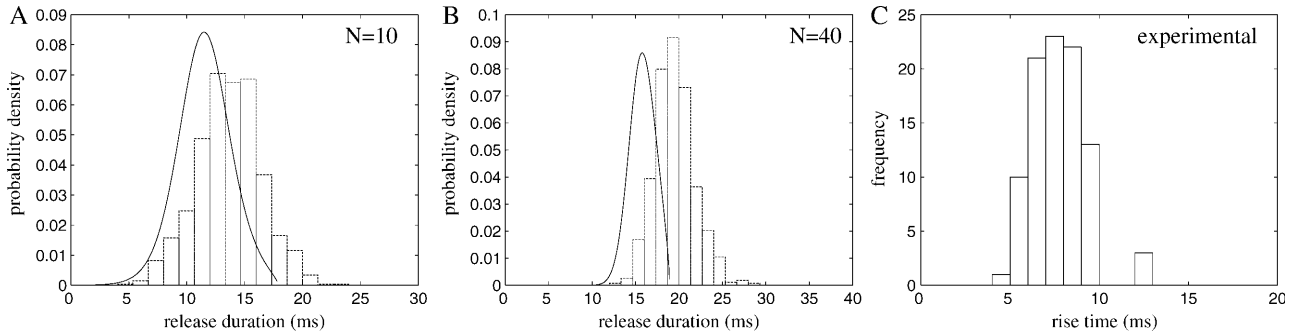

FIGURE 5 Distribution of spark durations for clusters containing (*A*) 10 RyRs and (*B*) 40 RyRs. The bars are a histogram of the results of a Monte Carlo simulation of the model and the line is the analytical result calculated using stochastic phase-plane analysis ($J_0 = 3.5$, $\rho = 0.2$, $r = 0.3$, and $\delta = 0.114$). The model results are compared with experimental measurements (*C*) of spark rise times (Wang et al., 2002).

attrition in terminating sparks as N is increased. In the section ''Stochastic phase-plane analysis'', we showed that the spark would terminate due to depletion of JSR Ca^{2+} when $J < J_c$. When $N = 10$, stochastic attrition causes the sparks to terminate before the JSR is depleted to the critical level J_c. However, when $N = 40$, the relative importance of stochastic attrition is decreased, and the dominant mechanism for spark termination is a partial depletion of the JSR Ca^{2+}. Fig. 5 *C* shows an experimental measurement of the distribution of rise times of sparks from a single hyperactive release site (Wang et al., 2002). This experimental result agrees with the model prediction. It has also been shown that the variation in rise time is not related to local SR Ca^{2+} filling (Wang et al., 2002), which agrees with the mechanism for spark variability presented in this article. It should be noted that although Wang et al. (2002) reported a variation in release durations, earlier studies had suggested that spark durations are highly stereotypical (Bridge et al., 1999).

Role of FKBP

In this section, the role of the FKBP is investigated using a previous model of coupled-gating (Sobie et al., 2002). Again, the aim of this calculation is to use mathematical analysis to explain why the behavior of the model changes. The RyRs in the cluster are coupled by a FKBP that modulates the ''opening'' and ''closing'' rates of each RyR. This model of coupled-gating is introduced by Eqs.11 and 12 (Sobie et al., 2002), and the strength of coupling is parameterized by the coupling constant k_{coup}. Fig. 6 shows the distribution of spark duration calculated for different coupling constants using a Monte Carlo simulation and stochastic phase-plane analysis. When the coupling factor (k_{coup}) is reduced to 0.6, the mean spark duration increases modestly from 18 ms to 23 ms (Fig. 6, *A* and *B*). However, when the coupling factor is reduced further to 0.2, the mean spark duration is greatly increased to 585 ms (Fig. 6 *C*) and the shape of the distribution is changed from a bell-shaped curve to a distribution with an exponentially decaying tail. This agrees with the previous model (Sobie et al., 2002) and experimental results. FK506 and rapamycin have been shown to reduce coupled-gating in planar lipid bilayer experiments (Marx et al., 2001). In experiments on isolated heart cells, it has been shown that these drugs increase the duration of Ca^{2+} sparks (Xiao et al., 1997; Lukyanenko et al., 1998; Sobie et al., 2002).

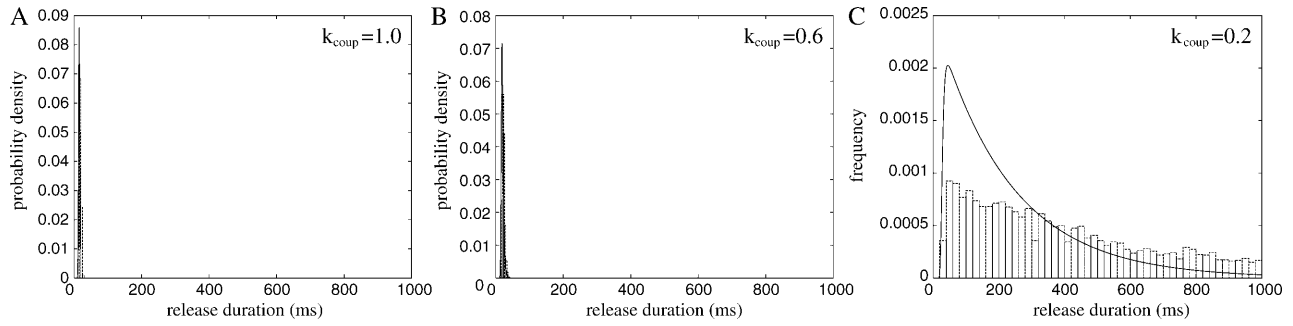

FIGURE 6 Distribution of spark durations as function of the RyR coupling constant (k_{coup}). (*A*) Normal coupling $k_{coup} = 1$, (*B*) partial reduction $k_{coup} = 0.6$, and (*C*) reduced coupling $k_{coup} = 0.2$. The bars are from a Monte Carlo simulation of the model and the line is the analytical result. Note that when k_{coup} is reduced below a threshold, the mean spark duration is greatly increased and the distribution changes from a bell shape to a distribution with a long (exponential) tail.

However, contradictory experimental results have been reported where FK506 ''only weakly modulated'' Ca^{2+} sparks (Soeller and Cannell, 2002). This model of coupled-gating gating gives a possible explanation of these contradictory results because the spark duration is only significantly increased when the coupling constant is reduced below a threshold value. The mathematical reason for this change in behavior can be understood by considering the phase-plane portrait when the coupling is interrupted (Fig. 7). During a spark with normal coupling between the RyRs (Fig. 7 *A*), the system moves down the nullcline from point *2* to *3*, where it will ''fall off'' the nullcline and the spark will terminate (if it has not already terminated due to a stochastic transition). Fig. 7 *B* shows that the system gains an extra fixed point (at point *3* in the figure) when the coupling constant k_{coup} is reduced below a critical value. During a spark with interrupted coupling between the RyRs (Fig. 7 *B*), the system moves down the nullcline from point *2* to the new fixed point at point *3*. It will remain at this point until a stochastic transition terminates the spark. The tail of the distribution is exponential because at the fixed point J is constant, therefore the rate of stochastic transitions is constant. The bifurcation between these two behaviors can be calculated by finding the critical point (ϕ_c, J_c) where the stable and unstable branches of the nullcline of ϕ join, thus.

$$\phi_c = \frac{\alpha - 1}{\alpha(1 + \rho k_{coup})} \quad \text{and} \quad J_c = \frac{\tilde{J}}{1 + \delta\tilde{J}}, \tag{30}$$

where

$$\tilde{J} = \frac{(1 + \rho k_{coup})\alpha}{\alpha - 1}\left(\frac{\rho k_{coup}(\alpha - 1)}{1 + \rho k_{coup}}\right)^{1/\alpha}, \tag{31}$$

and α is the exponent in the RyR transition coefficients. There will be a fixed point on $\phi_+(J)$ if the nullcline of J lies above this critical point (see Fig. 7 *B*). The fixed point of J at ϕ_c can be calculated using Eq. 17 and is

$$J_{c_J}(\phi_c) = \frac{J_0 r}{r + \phi_c} = \frac{J_0\alpha(1 + \rho k_{coup})r}{\alpha\rho k_{coup} r + \alpha - 1}, \tag{32}$$

where J_0 is the network SR Ca^{2+} and r is the rate of refill of the JSR from the network SR. If $J_{c_J} > J_c$ (i.e.. if $[Ca^{2+}]_{NSR}$ is too high), there will be a fixed–point on $\phi_+(J)$ which extends the duration of the spark. This implicit inequality for k_{coup} cannot be analytically inverted, but can be approximated given that $\rho, \delta \ll 1$. The bifurcation in behavior then occurs when $k_{coup} < k_c$ where

$$k_c \approx \frac{1}{\rho(\alpha - 1)}\left(\frac{J_0 r(\alpha - 1)}{\alpha - 1 + \alpha r}\right)^{\alpha}. \tag{33}$$

This formula tells us if the coupling constant k_{coup} is too small, then the sparks will be extended due to the existence of a fixed point on the stable nullcline of ϕ, thus explaining the model results (Fig. 6). Note that when $\alpha = 4$ and ρ is small, then $k_c \propto J_0^4$. The power of 4 tells us that the bifurcation point is very sensitive to value of J_0, which is proportional to $[Ca^{2+}]_{NSR}$.

DISCUSSION

In this article, a novel mathematical analysis has been applied to a model of Ca^{2+} release in cardiac myocytes. The dependency of spark frequency on $[Ca^{2+}]_{myo}$ and $[Ca^{2+}]_{JSR}$ was calculated, and showed that the spark frequency is very sensitive to the SR Ca^{2+} loading (Fig. 4). The spark frequencies were calculated for models containing RyRs with different Hill constants for Ca^{2+} activation. It was demonstrated that if the Hill constant was reduced from 4 to 3, the spark frequency increased by a factor of 10^3. The low frequency of Ca^{2+} sparks in healthy cardiac cells suggests that the effective Hill coefficient for RyR in cardiac myocytes is 4.

The distribution of spark durations was calculated using the technique of stochastic phase-plane analysis, which allowed the relative importance of the stochastic and

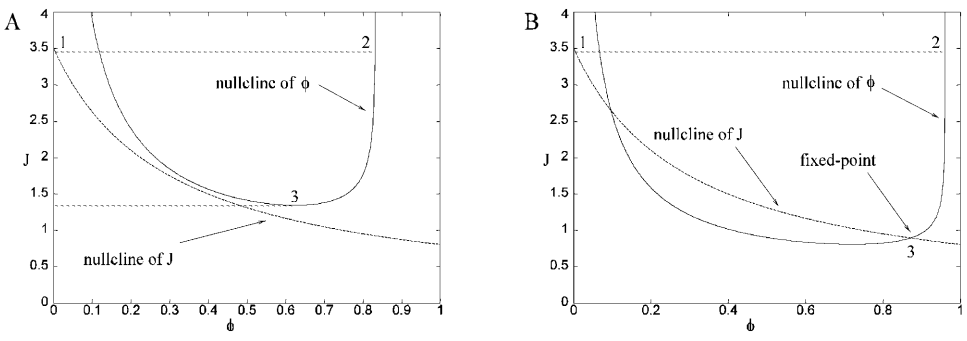

FIGURE 7 Phase-plane and null-clines of the model when (*A*) normal coupling ($k_{coup} = 1$) and (*B*) interrupted coupling ($k_{coup} = 0.2$). The nullcline for ϕ is the stationary point on the chain when J is fixed. Point *1* (in both phase portraits) is the stable fixed point the system is in before a spark has been generated. When a spark is generated the system jumps to point *2* and then moves down the nullcline toward point *3*. The system can make a stochastic transition from the nullcline ϕ_+ to $\phi = 0$. With normal coupling (*A*), the system ''falls off'' the nullcline at *3*, terminating the spark if it has not already been terminated by a stochastic transition. With interrupted coupling (*B*), the system reaches a fixed point at *3* so it does not ''fall off'' the nullcline at this point. However, eventually the spark will terminate due to a stochastic transition. Since J is constant at the fixed point, the rate of transitions from the fixed point is constant and the tail of the distribution of spark durations is exponential.

deterministic mechanisms to be examined. It was shown that when the number of RyRs in the CaRU was increased from 10 to 40 (keeping the maximum combined current through all RyRs constant), the mean spark duration increased and the width of the distribution of spark lengths was reduced. This demonstrates how the role of stochastic attrition in terminating spark is reduced as the number of RyRs in the cluster is increased. Stochastic attrition is necessary to explain the experimentally observed distribution of Ca^{2+} release times (Wang et al., 2002). The deterministic mechanism by which sparks were terminated was partial depletion of the $[Ca^{2+}]_{JSR}$. When the $[Ca^{2+}]_{JSR}$ fell below a critical value, the spark terminated because the local positive feedback loop was not sufficiently strong to maintain release. This critical value of $[Ca^{2+}]_{JSR}$ (typically $\sim$1/3 of the resting concentration) is substantially larger than total depletion, and is increased due to the sensitivity of the RyR on $[Ca^{2+}]_{JSR}$ (Terentyev et al., 2002). The model predictions are qualitatively robust to parameter changes, providing the approximations used in the mathematical analysis are kept. These are that $\varepsilon_{ds}, \varepsilon_B, \varepsilon_m, \varepsilon_{JSR} \ll 1$ (which are easily satisfied by the biophysical parameters), $1 > J_c/J_0 \approx 0.3$, and $1 \ll \tau_{JSR} \approx 15$ (see Eq. 15). If $J_c/J_0 > 1$, the model would be unable to sustain sparks, and if $J_c/J_0 \ll 1$ then sparks would only terminate if the $[Ca^{2+}]_{JSR}$ was totally depleted. If $\tau_{JSR} \approx 1$, then stochastic transitions would be less important and the distribution of spark durations would be approximately uniform.

The role of the FK-binding protein that couples the RyRs was examined using an established model for this process (Sobie et al., 2002). When the RyR coupling factor (k_{coup}) was reduced below a threshold level (k_c), the distribution of the spark durations changed from a bell-shaped curve of mean 18 ms to an approximate exponential distribution of mean >100 ms (Fig. 6). This model prediction agrees with experiments where the FK-binding protein is interrupted with FK506. The analysis showed that this dramatic change in distribution was due to the creation of a new fixed point when $k_{coup} < k_c$. An approximate calculation of k_c showed that it is proportional to the SR Ca^{2+} loading to the power of 4. This large power tells us that k_c is very sensitive to SR Ca^{2+} loading, and suggests that the effect of FK506 on increasing spark lengths can be reversed by a small reduction in SR loading. This could easily be tested experimentally by first treating cells with FK506, then applying a low dose of cyclopiazonic acid (a SERCA inhibitor) to see if the effect of the FK506 on sparks is reversed.

The model of sparks analyzed in this article is similar to most previous models of local Ca^{2+} release, which include a large number of stochastic RyRs in a single release unit (Stern, 1992; Stern et al., 1999; Sobie et al., 2002; Greenstein and Winslow, 2002). One feature that all these models share is that they display strong local feedback, so that the majority of channels (which have not be inactivated) are either all open or all closed. This feature of the models is not contradicted by experimental results, which put a lower bound of 18 RyRs involved in the generation of each spark (Bridge et al., 1999). A recent experimental result has shown that a single opening of LCC can lead to 4–6 RyRs generating a spark (Wang et al., 2001). This suggests that there is a strong coupling between each LCC and a small group of RyRs in the cluster (this feature is incorporated in the model of Greenstein and Winslow, 2002). This result does not necessarily contradict this model of spontaneous Ca^{2+} sparks. For example, in a cluster containing 60 RyRs ($[Ca^{2+}]_{myo} = 100$ nM and $[Ca^{2+}]_{JSR} = 0.8$ mM) and 4 RyRs are opened, then the probability of all the other receptors opening within the next 100 ms is just 15%.

In the fire-diffuse-fire model for Ca^{2+} waves, regenerative waves occur when Ca^{2+} from a spark at one CaRU diffuses to a neighboring CaRU, where it triggers further release (which then diffuses to a neighboring CaRU and so on). The model suggests that sparks occur before waves. Experiments on Ca^{2+} overloaded cells have shown that cells can exhibit sparks and waves, only spark, or only waves. The stochastic model of Ca^{2+} sparks in this article suggests a possible explanation for these different cases. Assume that between spontaneous Ca^{2+} waves the myoplasmic Ca^{2+} is approximately constant and the SR Ca^{2+} (J) increases slowly. The spark frequency will increase as the SR Ca^{2+} increases (see Fig. 4). Fig. 8 is a schematic diagram of the spark separation of a single CaRU as a function of SR Ca^{2+} for different local $[Ca^{2+}]_{myo}$. For sparks to be observable, the spark separation must be below a critical value T_s at resting $[Ca^{2+}]_{myo}$, which occurs when $[Ca^{2+}]_{SR}$ rises above J_s. When Ca^{2+} is released from one CaRU, it diffuses to neighboring CaRUs, which increases the local $[Ca^{2+}]$ at neighboring CaRUs for the duration of the spark, and thus increases the rate of spark generation (the *lower lines* in Fig. 8). If the mean spark separation (T_w) is less than mean length of a spark, then there is a high probability of further Ca^{2+} release and a regenerative wave propagating. This will occur if $[Ca^{2+}]_{SR}$ is above a critical value J_w. The occurrence of sparks and waves can be explained by the relative values of J_w, J_s, and the equilibrium SR Ca^{2+} J_0:

1. $J_0 < J_s$ and $J_0 < J_w$, then no sparks and no waves.
2. $J_s < J_0$ and $J_0 < J_w$, then sparks but no waves (Fig. 8 *A*).
3. $J_s < J_w$ and $J_w < J_0$, then sparks and waves (Fig. 8 *A*).
4. $J_w < J_0$ and $J_w < J_s$, then waves but no sparks (Fig. 8 *B*).

The last case is not a contradiction; it just means that any spark will trigger a wave, so individual sparks will not be observed. The difference between case 3 and case 4 is that in case 4, after a spark is generated, the myoplasmic Ca^{2+} in the neighborhood of surrounding CaRUs rises by more than in case 3. This can be examined experimentally by

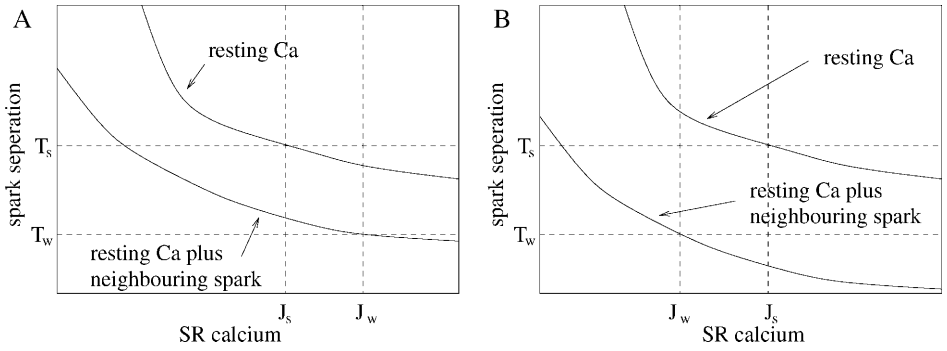

FIGURE 8 Schematic graph of the spark separation of a single CaRU as a function of $[Ca^{2+}]_{SR}$ (see Fig. 4 for the actual model calculation). Each graph shows the spark separation for resting Ca^{2+}, and the spark separation for the local $[Ca^{2+}]_{myo}$ at a CaRU while a spark is occurring at a neighboring CaRU. J_s is the level of SR Ca^{2+} required for the spark separation to be sufficiently small for sparks to be observed. J_w is the level of SR Ca^{2+} needed for a wave to be generated. *A* shows the case when both sparks and waves occur because $J_s < J_w$. *B* shows the case when only waves occur because $J_s > J_w$.

introducing a transmembrane Ca^{2+} buffer, which would reduce the gain in Ca^{2+} at neighboring CaRUs after a spark is generated.

APPENDIX 1: STOCHASTIC TRANSITIONS

The expressions for the fixed-point first passage times will now be calculated. A full derivation and discussion can be found in Hinch (2002). Consider an $N + 1$ state continuous time Markov chain where the system can only jump to neighboring positions on the chain. Define ϕ as the relative position on the Markov chain ($\phi = n/N$). The rate of transitions from the n to $n + 1$ position is the jump function $f(\phi)$, and the rate of transitions from the n to $n - 1$ position is the jump function $g(\phi)$. A stationary point on the chain is one where $f(\phi) = g(\phi)$. We shall consider jump functions such that the chain has two stable fixed points ($\phi_\pm$) and one unstable fixed point (ϕ_0), such that $\phi_- < \phi_0 < \phi_+$.

Stationary distribution

The first part of the analysis is to calculate the stationary distribution of the Markov chain in the limit of a large number of states ($N \nearrow \infty$). Define p_n as the probability the system is in the n^{th} position on the chain in the stationary distribution. The stationary distribution is calculated using the principle of detailed balance (Grimmett and Stirzaker, 2001)

$$p_n = p_k \prod_{i=k+1}^{n} \frac{f((n-1)/N)}{g(n/N)}, \\ = p_k \exp\left(\sum_{i=k+1}^{n} \ln\left(\frac{f((n-1)/N)}{g(n/N)} \right) \right), \quad (34)$$

where $0 \le k < n$. The functions $f(\phi)$ and $g(\phi)$ are smooth. Additionally, with the exception of the limit where $\phi \to 0$ and $\phi \to 1$ (see below for alterations in analysis in this case), the second derivatives of $\ln(f(\phi))$ and $\ln(g(\phi))$ are bounded. Therefore the sums can be approximated using the trapezium rule (Priestley, 1997)

$$\sum_{i=k}^{n} \ln(f(n/N)) = \frac{\ln(f(k/N)) + \ln(f(n/N))}{2} \\ + N \int_{k/N}^{n/N} \ln(f(\phi)) d\phi + O(1/N). \quad (35)$$

Inserting this into Eq. 34 gives

$$p_{N\phi} = \frac{A}{\sqrt{f(\phi)g(\phi)}} \exp(-NV(\phi)), \quad (36)$$

where $V(\phi)$ is the ''derived potential''

$$V(\phi) = \int^{\phi} \ln\left(\frac{g(\phi')}{f(\phi')} \right) d\phi' \quad (37)$$

and A is a constant. The value of A is then chosen to satisfy the normalization condition

$$\sum_{i=0}^{N} N p_i = 1. \quad (38)$$

The asymptotic approximation of $p_{N\phi}$ (Eq. 36) shows excellent agreement with the stationary distribution of the Markov chain calculated using Monte Carlo numerical simulations (Hinch, 2002). The analysis needs to be modified when we consider a Markov chain where the maximum of $p_{N\phi}$ lies on the boundary $n = \phi = 0$, and either $f(\phi)$ or $g(\phi)$ are proportional to ϕ in the limit $\phi \to 0$. This is the case when we are considering spark generation. The problem arises because $\ln(g(\phi)/f(\phi))$ diverges logarithmically in the limit $\phi \to 0$, so that the trapezium rule is invalid. After taking this correction into account we find

$$p_{N\phi} = \frac{p_0 \Gamma f(0)}{g(1/N)} \sqrt{\frac{f(1/N)g(1/N)}{f(\phi)g(\phi)}} \exp(-N(V(\phi) - V(1/N))) \\ \text{when } \phi \ge 1/N, \quad (39)$$

where $\Gamma \approx 1$ and depends on the exact form of $f(\phi)$ and $g(\phi)$. $\Gamma(\phi)$ can be calculated by considering the difference between using Stirling's formula and the trapezium rule to estimate the factorial function. In the spark model when $\varepsilon_m N/J_0 (\approx 0.1) \ll 1$, then $\Gamma \approx (\sqrt{2\pi}/e)^{\alpha-1}$.

Unstable fixed-point dynamics

The next part of the analysis is to consider the approximate dynamics of the system in the region of the unstable fixed point. The stationary distribution $p_{N\phi}$ will be two bell-shaped distributions centered on ϕ_- and ϕ_+, separated by a minimum at ϕ_0 (see Fig. 9 *A*). The state space ϕ can be separated into three regions: $R_\pm$ centered on $\phi_\pm$ and R_0 centered on ϕ_0. In the limit $N \nearrow \infty$, the width of the region R_0 in ϕ is $O(1/\sqrt{N})$. The aim of the analysis is to calculate the first passage times between the regions $R_\pm$; note that during one of these transitions, the system must go through the region R_0 since only nearest neighbor jumps are allowed. Fig. 9 *B* shows a sample time series of the position on the chain calculated using a Monte Carlo simulation. The

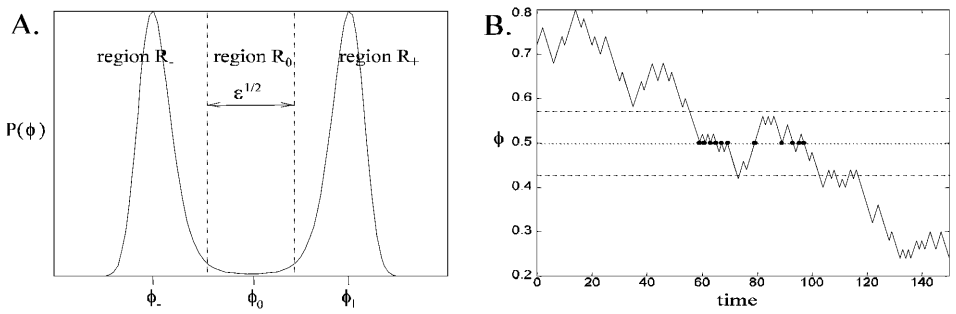

FIGURE 9 (*A*) Stationary distribution of a Markov chain model with stable stationary points at $\phi_\pm$ and an unstable stationary position ϕ_0. The state space is split into three regions, $R_\pm$ and R_0, centered about the stationary points. The width of the region R_0 is $O(\sqrt{\varepsilon})$, where $\int = 1/N$. (*B*) Monte Carlo simulation of a time series of a Markov model with two stable and one unstable stationary points. Note that the system visits the unstable stationary position (at $\phi_0 = 0.5$) many times (marked with *blobs*) before leaving the region R_0.

functions $f(\phi)$ and $g(\phi)$ are chosen such that the chain has stable stationary points at $\phi_- = 0.25$ and $\phi_+ = 0.75$, and an unstable stationary point at $\phi_0 = 0.5$. The figure shows the system undergoing a transition from the region of R_+ to R_-. Note that the system remains in the region R_0 for a short period of time, revisiting the unstable stationary position ϕ_0 many times (shown as blobs in Fig. 9 *B*). The task of this section is to calculate the mean number of times the system visits the unstable stationary position each time it enters the region R_0. To achieve this, we must calculate the dynamics of the Markov chain each time the system enters the region R_0. Define the small parameter $\varepsilon = 1/N$. As mentioned earlier, the width of the region R_0 in ϕ is $O(\sqrt{\varepsilon})$ (see Fig. 9 *B*); therefore in this region we can Taylor expand the functions $f(\phi)$ and $g(\phi)$ about ϕ_0. Define m as the number of positions on the chain the system is from the unstable stationary position ϕ_0, so when $m = 0$, the system is in the unstable stationary position. When the system is in the m^{th} state, the probability that the next jump on the chain is to the $m + 1$ position (i.e., a jump to the right) is

$$R_{\mathrm{m}} = \frac{f(\phi_0 + m/N)}{f(\phi_0 + m/N) + g(\phi_0 + m/N)} = \frac{1}{2} + \frac{\mu m}{2} + O(\mu^2), \tag{40}$$

where

$$\mu = -\frac{\gamma_0 \varepsilon}{2} \quad \text{and} \quad \gamma_0 = \frac{g'(\phi_0) - f'(\phi_0)}{f(\phi_0)}. \tag{41}$$

Note that since ϕ_0 is an unstable stationary position then $\mu > 0$ (the condition for ϕ_0 to be unstable is $g'(\phi_0) < f'(\phi_0)$). Therefore, when $m > 0$, the probability that the next jump is away from the unstable state if $>1/2$. The probability that the next jump on the chain is to the $m - 1$ position is L_{m}, which can be calculated using the fact that $L_{\mathrm{m}} + R_{\mathrm{m}} = 1$. Next, define Q_{m} as the probability that the system returns to $m = 0$ when it is in the mth position. During the following calculation, we shall consider the case $m \geq 0$; however, when $m < 0$, the leading order solution is the same. The partition theorem can be used to write a difference equation for Q_{m}:

$$Q_{\mathrm{m}} = R_{\mathrm{m}} Q_{\mathrm{m}+1} + L_{\mathrm{m}} Q_{\mathrm{m}-1}, \tag{42}$$

with boundary conditions $Q_0 = 1$ and $Q_\infty = 0$. Inserting the expansions for R_{m} and L_{m} (Eq. 40) yields

$$Q_{\mathrm{m}+1} - 2Q_{\mathrm{m}} + Q_{\mathrm{m}-1} + \mu m (Q_{\mathrm{m}+1} - Q_{\mathrm{m}-1}) + O(\mu^2) = 0. \tag{43}$$

This difference equation can be approximated by a differential equation in the limit $\mu \searrow 0$. Rescale the variable $x = \sqrt{\mu} m$ and introduce the continuous function $q(x) = Q_{\mathrm{m}}$. The rescaling of m allows the difference terms $Q_{\mathrm{m}\pm1}$ to be expanded about Q_{m} to give

$$Q_{\mathrm{m}\pm1} = q(x \pm \sqrt{\mu}) = q(x) \pm \sqrt{\mu}\frac{dq}{dx} + \frac{\mu}{2}\frac{d^2 q}{dx^2} + O(\mu^{3/2}). \tag{44}$$

Inserting this expansions into the difference Eq. 43 yields

$$\frac{d^2 q}{dx^2} + 2x\frac{dq}{dx} + O(\sqrt{\mu}) = 0, \tag{45}$$

with solution

$$q(x) = 1 - \mathrm{erf}(x) + O(\sqrt{\mu}) \quad \text{when} x > 0. \tag{46}$$

Here $\mathrm{erf}(x)$ is the standard error functions. The same calculation can be repeated for the case when $x < 0$. After each visit to the $m = 0$ position, the next jump must be to either the $m = +1$ or $m = -1$ position with equal probabilities. Therefore the probability that the system returns to the $m = 0$ position after leaving it is $(Q_1 + Q_{-1})/2$, and the probability that the system leaves the region R_0 is $1 - (Q_1 + Q_{-1})/2$. Define n_{return} as the mean number of times the system returns to the $m = 0$ position, then

$$n_{\text{return}} = \frac{1}{1 - (Q_1 + Q_{-1})/2} \approx \sqrt{\frac{\pi N}{-2\gamma_0}}. \tag{47}$$

Note that as N increases, the number of times the system visits the unstable stationary point ϕ_0 increases like $\sqrt{N}$. This asymptotic approximation can be checked using Monte Carlo simulations and both calculations are in excellent agreement (Hinch, 2002).

Stochastic fixed-point transitions

The final task is to combine the results of the previous sections to calculate the mean first passage times between the regions $R_\pm$. Define τ_+ as the first passage time from the R_+ region to the R_- region, and τ_- as the first passage time from R_- to R_+. The analysis presented in this section will calculate the leading order asymptotic approximation or $\tau_\pm$ in the limit $N \nearrow \infty$. The arguments presented below are only valid for the leading order term, and more care is needed if correction terms are to be calculated (Hinch, 2002). During each transition between the regions $R_\pm$, the system must pass through the region R_0. Define τ_{R_0} as the mean time between visits to the region R_0. The probability that the system is at the unstable stationary position is $p_{\mathrm{N}\phi_0}$. The mean time spent in this position during each visit is $1/2f(\phi_0)$ (remember $f(\phi_0) = g(\phi_0)$). Therefore the mean time between visits to the unstable stationary position is $1/2f(\phi_0)p_{\mathrm{N}\phi_0}$. However, each time the system is in the region R_0, it visits the unstable position (ϕ_0) on average n_{return} times. Therefore the mean time between visiting the region R_0 is

$$\tau_{R_0} = \frac{n_{\text{return}}}{2p_{N\phi_0} f(\phi_0)}. \quad (48)$$

When the system enters the unstable position ϕ_0, it does not ''remember'' whether it previously came from the region R_+ or R_- because it is a Markov process. Additionally (to leading order), after leaving ϕ_0, it is equally as likely to go to either the R_+ or R_- region. Therefore the probability that a transition occurs when the system enters the region R_0 is 1/2, so the mean time between transitions is $2\tau_{R_0}$. Finally we calculate the ratio of the mean first passage times $\tau_\pm$. This is achieved by considering the stationary distribution. Define $P_\pm$ as the probability that the system is in the regions $R_\pm$, which are calculated by summing the stationary distribution over the regions

$$P_- = \sum_{k=0}^{N\phi_0} p_k \quad \text{and} \quad P_+ = \sum_{k=N\phi_0}^{N} p_k. \quad (49)$$

Remember the time spent in the region R_0 is exponentially small, so it can be ignored in this asymptotic calculation. If $\phi_- \neq 0$ and $\phi_+ \neq 1$, then these sums can be approximated in the limit $N \nearrow \infty$ by integrals that can then be approximated using Laplace's method to give

$$P_\pm = \frac{A}{f(\phi_\pm)}\sqrt{\frac{2\pi N}{\gamma_-}}\exp(-NV(\phi_\pm)) + O(N^{-1/2}), \quad (50)$$

where $V(\phi)$ is the ''derived potential'' (Eq. 37) and $\gamma_\pm$ is defined by Eq. 41. Note that the normalization constant A can now be calculated using the fact that $P_+ + P_- \approx 1$. The ratio of the first passage times is then given by

$$\frac{\tau_+}{\tau_-} = \frac{P_+}{P_-}. \quad (51)$$

A transition from the region R_- to R_+ must be followed by a transition from R_+ to R_-; therefore the mean transition time is $(\tau_+ + \tau_-)/2$. Finally, combining Eqs. 36, 47, 48, 50, and 51 yields

$$\tau_\pm = \exp(N\Delta V_\pm)\left(\frac{2\pi N}{f(\phi_\pm)\sqrt{-\gamma_0\gamma_\pm}} + O(1)\right), \quad (52)$$

where $\Delta V_\pm = V(\phi_0) - V(\phi_\pm)$. This equation is used in the section ''Stochastic fixed-point transitions'' to calculate the rate of spark termination. The calculation of the rate of spark generation is slightly more complicated since the maximum of the stationary distribution is in the $n = 0$ position. Equation 39 for the stationary distribution must be used instead of Eq. 36, then

$$\tau_{\text{gen}} = \exp(N\Delta V_-) \times \left(\frac{g(1/N)\sqrt{2\pi N}}{\Gamma f(0)\sqrt{-\gamma(\phi_-)f(1/N)g(1/N)}} + O(1/\sqrt{N})\right), \quad (53)$$

where $\Delta V_- = V(\phi_0) - V(1/N)$. This equation is used to calculate spark frequencies in the section ''Stochastic fixed-point transitions''.

APPENDIX 2: GLOSSARY OF PARAMETERS AND BIOPHYSICAL ESTIMATES

Table 1 is a glossary of the parameters used in the model and the values used. The values are estimates taken from the biophysical literature and the references are: V_{ds} and A_{ds} were calculated by assuming that the diadic space is a cylinder of width 10 nm and radius 200 nm (Frank, 1990). V_{cell} (Greenstein and Winslow, 2002), V_{JSR} (Sobie et al., 2002), and D_{Ca} (Allbritton et al., 1992; Zhou and Neher, 1993). l_{eff} will be a bit larger than the width of the diadic space and $g_D \approx D_{Ca}A_{ds}/l_{eff}$. $[Ca^{2+}]_{NSR}$ (Sobie et al., 2002), $[B]_{tot}$ (Sobie et al., 2002), K_B (Rice et al., 1999), $[CSQ]_{tot}$ (Greenstein and Winslow, 2002), and K_{CSQ} (Greenstein and Winslow, 2002). The simplification is made that β_{JSR} is approximately constant, and is calculated using Eq. 6 with an ''effective'' JSR concentration during a spark of 360 μM. A cell contains typically 50,000 LCC (Rose et al., 1992; McDonald et al., 1986) and each CaRU contains typically 4 LCC (Greenstein and Winslow, 2002); therefore, $N_{CaRU} \approx 12{,}500$. The myoplasmic volume per CaRU is then 2 μm^3. J_{max} is calculated by considering the Ca^{2+} release from a single CaRU during E-C coupling: $[Ca^{2+}]$ rises by 1.0 μM in 10 ms (Wang et al., 2002) and typically 98% is buffered (Rice and Jafri, 2001). τ_{tr} (Greenstein and Winslow, 2002). α (Sobie et al., 2002). K_0 (average of Sobie et al., 2002, and Gyorke and Gyorke, 1998) with original data from Thedford et al. (1994), Cheng et al. (1996), Gyorke and Gyorke (1998), Lukyanenko et al. (1998), and Ching et al. (2000). τ_{open} (Gyorke and Gyorke, 1998). ρ estimated from single RyR recordings in Zahradnikova and Zahradnik (1996).

TABLE 1

Parameter	Definition	Value
V_{ds}	Volume of diadic space (ds)	1.26×10^{-3} μm^3
A_{ds}	Interface area of ds and myoplasm	1.26×10^{-2} μm^2
V_{cell}	Cell volume	25 pl
V_{JSR}	Volume of JSR	1.0×10^{-2} μm^3
D_{Ca}	Diffusion constant of Ca^{2+}	0.3 μm^2 ms^{-1}
l_{eff}	Effective diffusion length of Ca^{2+}	13.2 nm
g_D	Diffusive rate from ds	0.286 μm^3 ms^{-1}
$[Ca^{2+}]_{myo}$	Myoplasmic Ca^{2+} concentration	0.1 μM
$[Ca^{2+}]_{NSR}$	Network SR Ca^{2+} concentration	1000 μM
$[B]_{tot}$	Total buffer in ds	24 μM
K_B	Calmodulin dissociation constant	2.38 μM
$[CSQ]_{tot}$	Total calsequestrin in JSR	13.5 mM
K_{CSQ}	Calsequestrin dissociation constant	0.63 mM
β_{JSR}	Buffering factor in JSR	0.13
N_{CaRU}	Number of CaRU per cell	12500
J_{max}	Max. current from SR into CaRU	10 μM μm^3 ms^{-1}
τ_{tr}	Transfer time from NSR to JSR	3 ms
N	Number of RyRs in CaRU	10–100
α	Number of Ca^{2+} to activate RyR	4 (or 3)
K_0	RyR dissociation constant	10 μM
τ_{open}	Mean open time of RyR	0.5 ms
ρ	Proportion of time closed in H-mode	0.2
$\triangle$	Sensitivity of K_{RyR} on JSR Ca^{2+}	0.4 mM^{-1}

The nondimensional parameters are calculated from the physiological parameters using Eq. 15 and are listed in Table 2.

The author thanks Prof. D. Noble and Dr. A. Fowler for useful discussions relating to this manuscript.

TABLE 2

Parameter	Value
ε_{ds}	0.002
ε_B	0.002
ε_m	0.01
ε_{JSR}	0.03
J_0	3.5
τ_{JSR}	15
r	0.3
ρ	0.2
δ	0.114

This work was supported by the British Heart Foundation and the Wellcome Trust.

REFERENCES

Allbritton, N. L., T. Meyer, and L. Stryer. 1992. Range of messenger action of Ca^{2+} ion and inositol 1,4,5-triphosphate. *Science*. 258:1812–1815.

Aptel, H., and N. Freestone. 1998. Correlation between Ca^{2+} waves, Ca^{2+} sparks and the loading state of the sarcoplasmic reticulum in rat ventricular cardiomyocytes. *J. Physiol.* 509P:155P. (Abstr.)

Bassani, J. W. M., W. Yuan, and D. M. Bers. 1995. Fractional SR Ca^{2+} release is regulated by trigger Ca^{2+} and SR Ca^{2+} content in cardiac myocytes. *Am. J. Physiol. Cell Physiol.* 268:C1313–C1319.

Bridge, J. H. B., P. R. Ershler, and M. B. Cannell. 1999. Properties of Ca^{2+} sparks evoked by action potentials in ventricular myocytes. *J. Physiol.* 518:469–478.

Cheng, H., M. B. Cannell, and W. J. Lederer. 1994. Propagation of excitation-contraction coupling into ventricular myocytes. *Pflugers Arch.* 428:415–417.

Cheng, H., W. J. Lederer, and M. B. Cannell. 1993. Ca^{2+} sparks: elementary events underlying excitation-contraction coupling in heart muscle. *Science*. 262:740–744.

Cheng, H., M. R. Lederer, W. J. Lederer, and M. B. Cannell. 1996. Ca^{2+} sparks and Ca^{2+} waves in cardiac myocytes. *Am. J. Physiol. Cell Physiol.* 270:C148–C159.

Ching, L. L., A. J. Williams, and R. Sitsapesan. 2000. Evidence for Ca^{2+} activation and inactivation sites on the luminal side of the cardiac ryanodine receptor complex. *Circ. Res.* 87:201–206.

Frank, J. S. 1990. Ultrastructure of the unfixed myocardial sarcolemma and cell surface. *In* Ca^{2+} and the Heart. G. A. Langer, editor. Raven Press, New York. 1–25.

Franzini-Armstrong, C., F. Protasi, and V. Ramesh. 1998. Comparative ultrastructure of Ca^{2+} release units in skeletal and cardiac muscle. *Ann. N. Y. Acad. Sci.* 853:20–30.

Franzini-Armstrong, C., F. Protasi, and V. Ramesh. 1999. Shape, size, and distribution of Ca^{2+} release units and couplons in skeletal and cardiac muscles. *Biophys. J.* 77:1528–1539.

Greenstein, J. L., and R. L. Winslow. 2002. An integrative model of the cardiac ventricular myocyte incorporating local control of Ca^{2+} release. *Biophys. J.* 83:2918–2945.

Grimmett, G. R., and D. R. Stirzaker. 2001. Probability and Random Processes, 3rd ed. Oxford University Press, Oxford.

Gyorke, S., and M. Fill. 1993. Ryanodine receptor adaptation: control mechanism of Ca^{2+}-induced Ca^{2+} release in the heart. *Science.* 260:807–809.

Gyorke, I., and S. Gyorke. 1998. Regulation of the cardiac ryanodine receptor by luminal Ca^{2+} sensing sites. *Biophys. J.* 75:2801–2810.

Hinch, R. 2002. Mathematical models of the heart. *DPhil thesis*. Oxford University, UK.

Keener, J., and J. Sneyd. 1998. Mathematical Physiology. Springer-Verlag, New York.

Kramers, H. A. 1940. Brownian motion in a field of force and the diffusion model of chemical reactions. *Physica*. 7:284–304.

Lederer, W. J., E. Niggli, and R. W. Hadley. 1990. Na^{+}-Ca^{2+} exchange in excitable cells: fuzzy space. *Science*. 248:283.

Marx, S. O., J. Gaburjakova, M. Gaburjakova, C. Henrikson, K. Ondrias, and A. R. Marks. 2001. Coupled gating between cardiac Ca^{2+} release channels (ryanodine receptors). *Circ. Res.* 88:1151–1158.

Lopez-Lopez, J. R., P. S. Shacklock, C. W. Balke, and W. G. Wier. 1994. Local stochastic release of Ca^{2+} in voltage-clamped rat heart cells: visualization with confocal microscopy. *J. Physiol.* 480:21–29.

Lukyanenko, V., T. F. Wiesner, and S. Gyorke. 1998. Termination of Ca^{2+} release during Ca^{2+} sparks in rat ventricular myocytes. *J. Physiol.* 507:667–677.

McDonald, T. F., A. Cavalie, W. Trautwein, and D. Pelzer. 1986. Voltage-dependent properties of macroscopic and elementary Ca^{2+} channel currents in guinea pig ventricular myocytes. *Pflugers Arch.* 406: 437–448.

Nabauer, M., and M. Morad. 1990. Ca^{2+}-induced Ca^{2+} release as examined by photolysis of caged Ca^{2+} in single ventricular myocytes. *Am. J. Physiol. Cell Physiol.* 258:C189–C193.

Negretti, N., A. Varro, and D. A. Eisner. 1995. Estimate of net Ca^{2+} fluxes and sarcoplasmic reticulum Ca^{2+} content during systole in rat ventricular myocytes. *J. Physiol.* 486:581–591.

Niggli, E., and W. J. Lederer. 1990. Voltage-independent Ca^{2+} release in heart muscle. *Science*. 250:565–568.

Priestley, H. A. 1997. Introduction to Integration. Oxford University Press, New York.

Rice, J. J., and M. S. Jafri. 2001. Modelling cardiac Ca^{2+} handling. *Phil. Trans. R. Soc. Lond. A.* 359:1143–1157.

Rice, J. J., M. S. Jafri, and R. L. Winslow. 1999. Modeling gain and gradedness of Ca^{2+} release in the functional unit of the cardiac diadic space. *Biophys. J.* 77:1871–1884.

Rose, W. C., C. W. Balke, W. G. Wier, and E. Marban. 1992. Macroscopic and unitary properties of physiological ion flux through L-type Ca^{2+} channels in guinea-pig hearts. *J. Physiol. (Lond.).* 489:337–348.

Shacklock, P. S., W. G. Wier, and C. W. Balke. 1995. Local Ca^{2+} transients (Ca^{2+} sparks) originate at transverse tubules in rat heart cells. *J. Physiol.* 487:601–608.

Sham, J. S. K., L. S. Song, Y. Chen, L. H. Deng, M. D. Stern, E. G. Lakatta, and H. Cheng. 1998. Termination of Ca^{2+} release by a local inactivation of RyRs in cardiac myocytes. *Proc. Natl. Acad. Sci. USA.* 98:15096–15101.

Sobie, E. A., K. W. Dilly, J. dos Santos Cruz, W. J. Lederer, and M. S. Jafri. 2002. Termination of cardiac Ca^{2+} sparks: an investigative mathematical modeling of Ca^{2+}-induced Ca^{2+} release. *Biophys. J.* 83: 59–78.

Soeller, C., and M. B. Cannell. 1997. Numerical simulation of local Ca^{2+} movements during L-type Ca^{2+} channel gating in the cardiac diad. *Biophys. J.* 73:97–111.

Soeller, C., and M. B. Cannell. 2002. A numerical study of ryanodine receptor gating in the cardiac diad and comparison with experimental data. *Biophys. J.* 84:432a. (Abstr.)

Stern, M. D. 1992. Theory of excitation-contraction coupling in cardiac muscle. *Biophys. J.* 63:497–517.

Stern, M. D., L. S. Song, H. Cheng, J. S. Sham, H. T. Yang, K. R. Boheler, and E. Rios. 1999. Local control models of cardiac excitation-contraction coupling. A possible role for allosteric interactions between cardiac myocytes. *J. Gen. Physiol.* 113:469–489.

Terentyev, D., S. Viatchenko-Karpinski, H. H. Valdivia, A. L. Escobar, and S. Gyorke. 2002. Luminal Ca^{2+} controls termination and refractory behavior of CICR in cardiac myocytes. *Circ. Res.* 91:414–420.

Thedford, S. E., W. J. Lederer, and H. H. Valdivia. 1994. Activation of sarcoplasmic reticulum Ca^{2+} release channels by intraluminal Ca^{2+}. *Biophys. J.* 66:A20. (Abstr.)

Valdivia, H. H., J. H. Kaplan, G. C. R. Ellis-Davies, and W. J. Lederer. 1995. Rapid adaptation of cardiac ryanodine receptors: modulation by Mg^{2+} and phosphorylation. *Science*. 267:1997–2000.

Varro, A., N. Negretti, S. B. Hester, and D. A. Eisner. 1993. An estimate of the Ca^{2+} content of the sarcoplasmic reticulum in rat ventricular myocytes. *Pflugers Arch.* 423:158–160.

Wagenknecht, T., M. Badermacher, R. Grassucci, J. Berkowitz, H. B. Xin, and S. Fleischer. 1997. Locations of calmodulin and FK506-binding protein on the three-dimensional architecture of the skeletal muscle ryanodine receptor. *J. Biol. Chem.* 272:32463–32471.

Wagner, J., and J. Keizer. 1994. Effects of rapid buffers on Ca^{2+} diffusion and Ca^{2+} oscillations. *Biophys. J.* 67:447–456.

Wang, S. Q., L. S. Song, E. G. Lakatta, and H. Cheng. 2001. Ca^{2+} signaling between single L-type Ca^{2+} channels and ryanodine receptors in heart cells. *Nature*. 410:592–596.

Wang, S. Q., L. S. Song, L. Xu, G. Meissner, E. G. Lakatta, E. Rios, M. D. Stern, and H. Cheng. 2002. Thermodynamically irreversible gating of ryanodine receptors in situ revealed by stereotyped duration of release of Ca^{2+} sparks. *Biophys. J.* 83:242–251.

Xiao, R. P., H. H. Valdivia, K. Bogdanov, C. Valdivia, E. G. Lakatta, and H. P. Cheng. 1997. The immunophilin FK506-binding protein modulates Ca^{2+} release channel closure in rat hearts. *J. Physiol.* 500: 343–354.

Xu, L., G. Mann, and G. Meissner. 1996. Regulation of cardiac Ca^{2+} release channel (ryanodine receptor) by Ca^{2+}, H^{+}, Mg^{2+} and adenine nucleotides under normal and simulated ischemic conditions. *Circ. Res.* 79:1100–1109.

Zahradnikova, A., and I. Zahradnik. 1996. A minimal gating model for the cardiac Ca^{2+} release channel. *Biophys. J.* 71:2996–3012.

Zhou, Z., and E. Neher. 1993. Mobile and immobile Ca^{2+} buffers in bovine adrenal chromaffin cells. *J. Physiol.* 469:245–273.